Biophysical Journal Volume 67 October 1994 1724–1732

Calorimetric Study of Crystal Growth of Ice in Hydrated Methemoglobin and of Redistribution of the Water Clusters Formed on Melting the Ice

Günter Sartor and Erwin Mayer
Institut für Allgemeine, Anorganische und Theoretische Chemie, Leopold-Franzens-Universität Innsbruck, A-6020 Innsbruck, Austria

ABSTRACT Calorimetric studies of the melting patterns of ice in hydrated methemoglobin powders containing between 0.43 and 0.58 (g water)/(g protein), and of their dependence on annealing at subzero temperatures and on isothermal treatment at ambient temperature are reported. Cooling rates were varied between ≈1500 and 5 K min^{-1} and heating rate was 30 K min^{-1}. Recrystallization of ice during annealing is observed at $T > 228$ K. The melting patterns of annealed samples are characteristically different from those of unannealed samples by the shifting of the melting temperature of the recrystallized ice fraction to higher temperatures toward the value of "bulk" ice. The "large" ice crystals formed during recrystallization melt on heating into "large" clusters of water whose redistribution and apparent equilibration is followed as a function of time and/or temperature by comparison with melting endotherms. We have also studied the effect of cooling rate on the melting pattern of ice with a methemoglobin sample containing 0.50 (g water)/(g protein), and we surmise that for this hydration cooling at rates of ≥≈150 K min^{-1} preserves on the whole the distribution of water molecules present at ambient temperature.

INTRODUCTION

In hydrated proteins a fraction of water of up to ≈0.3–0.4 (g water)/(g protein) remains mobile down to very low temperatures and does not crystallize even over long periods of time regardless of the rate of cooling or heating (for reviews see Kuntz and Kauzmann, 1974; Cooke and Kuntz, 1974; Finney, 1986; Rupley and Careri, 1991). Hydrated water above this hydration range crystallizes on slow cooling but can be vitrified with increasing rates of cooling. We recently reported a study by differential scanning calorimetry (DSC) on the vitrification and crystallization characteristics of freezable water in hydrated methemoglobin (MetHb), of between ≈0.4 and 0.7 (g water)/(g MetHb), which can be vitrified but crystallizes on heating (Sartor et al., 1992, 1993). One of the conclusions from this study was that the calorimetric glass→liquid transition and crystallization behavior of this vitreous but freezable water fraction is clearly different from that reported for "bulk" water (Johari et al, 1987; Hallbrucker et al., 1989), but very similar to that of water embedded in the pores of a synthetic hydrogel (Hofer et al., 1990).

We now extend the DSC study of hydrated MetHb powders and report here for the hydration range of 0.43–0.58 (g water)/(g MetHb) calorimetric evidence for recrystallization of ice at subzero temperatures and subsequent clustering of water on heating to ambient temperature, by using the shape of the melting endotherm of ice as indicator for these processes. We have systematically investigated the influence of cooling rate, annealing temperature, and annealing time on the shape of the melting endotherm and thereby obtained first for subzero temperatures values for the annealing temperature and/or time necessary for recrystallization of small ice crystals into larger ones. Second, after melting of these "large" ice crystals into "large" water clusters, we obtained for hydration water at ambient temperature an estimate of the time scale necessary for these clusters to redistribute and apparently equilibrate on the protein surface.

The endothermic features seen in the melting region of ice of the hydrated MetHb samples contain contributions from both the water and its interaction with the protein. For example, the melting point depression of ice in myoglobin solution has been analyzed by Doster et al. (1986) within the Flory/Huggins model. In this study we will use the shape of the melting endotherm and the peak maxima as sensitive indicators for ice crystal size distributions, and we will neglect contributions from the interaction with the protein because the emphasis here is on changes of the melting patterns upon annealing at a given temperature and/or time. We note that annealing of hydrated myoglobin powders at 250 K and subsequent changes in the shape of the melting endotherm of ice obtained by DSC have been reported by Doster et al. (1986), and that these changes have been interpreted in terms of partial transformation of a component II into a crystalline component I upon annealing.

MATERIALS AND METHODS

Hemoglobin from bovine blood (No. 51290, Fluka Chemical Corp., Buchs, Switzerland) was used in general except for the DSC curves of Fig. 4 where hemoglobin from human blood (No. H 7379, Sigma Chemical Co., St. Louis, MO) was used. Both were characterized in aqueous solution (phosphate-buffered at pH 6.8) by the UV-visible spectrum to be MetHb (Waterman, 1978) and used as received. MetHb was hydrated by keeping over saturated ammonium sulfate solution at a constant temperature over several weeks, following the description by Poole and Finney (1986) of preparation of solid-phase low-hydration samples. Water content of the as-received MetHb, determined by heating to 378 K, was 0.10 (g water)/(g MetHb). Final water content of hydrated MetHb was determined by weighing to ±0.01 mg, taking into account the water content of the as-received MetHb.

Received for publication 2 May 1994 and in final form 15 July 1994.

Address reprint requests to Dr. Erwin Mayer, Institut für Allgemeine, Anorganische und Theoretische Chemie, Leopold-Franzens-Universität Innsbruck, A-6020, Austria. Fax: 43 512 507 2934.

0006-3495/94/10/1724/09 $2.00

The hydrated samples were quickly crimp sealed into aluminum pans and weighed. The accuracy of the given hydration values is estimated to be ±0.02 (g water)/(g MetHb).

A differential scanning calorimeter (Model DSC-4, Perkin-Elmer Corp., Philadelphia, PA) with a selfwritten computer program for data acquisition was used for all studies. After the scans were taken, a baseline was subtracted to eliminate the curvature of the traces. The baseline was obtained by taking a scan with empty sample pans. The x and y data were imported to Origin, a computer program used to prepare the plots (MicroCal Software, Inc., Northampton, MA). Only crimp-sealed aluminum pans were used, to avoid evaporation losses and to obtain cooling rates of ≈150 K min^{-1} in the DSC instrument (Sartor et al., 1992). A cooling rate of ~1500 K min^{-1} was used for curve 1 of Fig. 5 by dipping the aluminum pan with sample into liquid N_2. The weights of the samples were between 14.10 and 21.44 mg. The temperature scales in the figures are not corrected for the thermal lag of the instrument (which is 1.5 for heating at a rate of 30 K min^{-1}), but the temperatures given in the text are corrected. Further experimental details on DSC are given by Sartor et al. (1992), Hofer et al. (1990), and Hallbrucker et al. (1989).

After several of the experiments, the UV-visible spectrum of MetHb dissolved in phosphate buffer (pH 6.8) was recorded again and found to be indistinguishable from that of the protein before exposure to the cooling/heating cycles. This is taken as evidence that no irreversible denaturation had occurred.

RESULTS

The DSC heating curves of Fig. 1 shown from 240 to 290 K were recorded using the same sample of hydrated MetHb powder, with 0.52 (g water)/(g MetHb), and they give an indication for the range of melting endotherm patterns of ice obtainable on heating the sample at 30 K min^{-1}. Curve 1 was obtained after cooling the sample in the DSC instrument from 295 to 103 K at a rate of ≈150 K min^{-1} and heating it to 295 K at 30 K min^{-1}. The melting endotherm consists of a broad asymmetric peak with a maximum at ≈265 K; a weak shoulder at ≈273 K indicates the melting of a small amount of another ice fraction. For curve 2 the sample was cooled from 295 to 103 K at ≈150 K min^{-1}, heated to 258 K at 30 K min^{-1}, annealed at 258 K for 60 min, cooled to 103 K, and reheated to 295 K at 30 K min^{-1} and its DSC scan recorded. The annealing temperature is marked in this and the following DSC curves with an arrow. The melting pattern was drastically changed in comparison with curve 1, and a large fraction of the ice now melted at a higher temperature, with a peak maximum of the intense sharp endotherm of 274 K, indicated by the broken line. However, a broad asymmetric peak with a maximum at ≈260 K and a shoulder at ≈270 K indicates the presence of two other size distributions of ice. For curve 3 the sample was cooled immediately after curve 2 from 295 to 103 K at ≈150 K min^{-1}, reheated, and its DSC scan recorded. For curve 4 the sample was kept at 295 K for 10 min after recording the DSC scan for curve 3, cooled thereafter to 103 K at ≈150 K min^{-1}, reheated and its DSC scan recorded. The intense peak centered at ≈273 K had disappeared, and the melting curve resembles that of curve 1. The area of the melting endotherms is for integration from 249 to 281 K 18.4 (curve 1), 18.9 (curve 2), 19.1 (curve 3), and 18.4 (curve 4) J/(g sample), respectively.

The change in melting pattern in going from curve 1 to curve 2 as an effect of annealing at subzero temperature is attributed to recrystallization of small ice crystals into larger ones. This effect is described by the Gibbs-Thomson equation (reviewed for ice by Pruppacher and Klett, 1980) and, for a given rate of heating, the melting point increases with increasing crystal size until it approaches that of the "bulk" crystal (Wunderlich, 1990). In curve 2 of Fig. 1 a shift to higher temperatures, toward the value of "bulk" ice, is clearly seen for a fraction of ice by the intense melting endotherm centered at 274 K, and possibly for a second fraction of ice by the shoulder at ≈270 K. The effects of annealing seen in curve 2 can be reduced by subsequent cooling and reheating (curve 3) and even more by keeping the sample for 10 min at 295 K (curve 4). The increase in area of the melting endotherms of curves 2 and 3, and the decrease for curve 4 to the value of curve 1, is consistent with this interpretation. We note that the effects of annealing seen in curve 2 can be reduced further and the shape of curve 1 approached by repeated cycles of cooling at ≈150 K min^{-1} and reheating of the sample at 30 K min^{-1} (not shown).

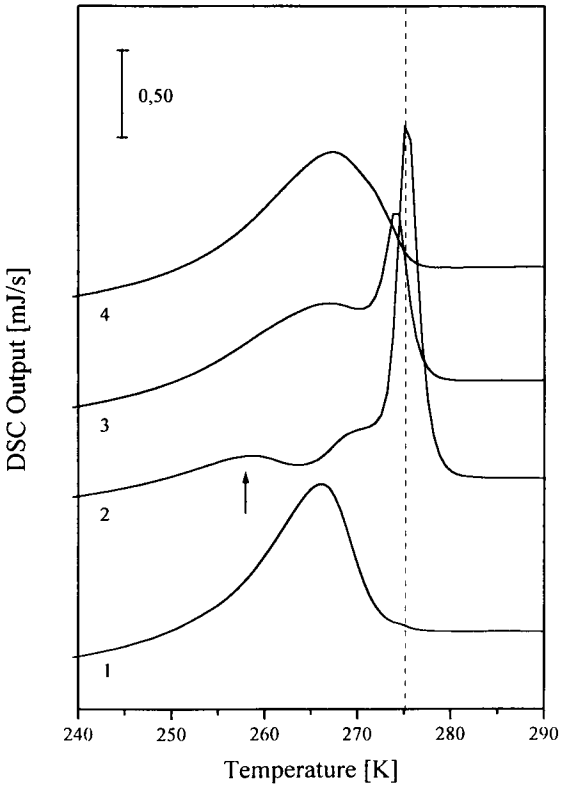

FIGURE 1 The DSC scans of the melting region of ice of a methemoglobin sample containing 0.52 (g water)/(g MetHb) for heating at a rate of 30 K min^{-1}. For curve 1 the sample was cooled from 295 to 103 K at ≈150 K min^{-1}, heated, and its DSC scan recorded. For curve 2 it was cooled thereafter from 295 to 103 K at ≈150 K min^{-1}, heated to 258 K at 30 K min^{-1}, annealed at 258 K for 60 min, cooled to 103 K, reheated to 295 K, and its DSC scan taken. For curve 3 the sample was cooled immediately after curve 2 from 295 to 103 K at ≈150 K min^{-1}, reheated, and its DSC scan recorded. For curve 4 the sample was kept thereafter at 295 K for 10 min, cooled to 103 K at ≈150 K min^{-1}, reheated, and its DSC scan recorded. The vertical broken line is at 275 K. In general, for Figs. 1–6, the curves are shifted vertically for clarity. The ordinate scales are for 1 mg sample weight. Annealing temperatures are marked by arrows. The temperature axes are not corrected for thermal lag of the instrument.

Fig. 2 shows in a systematic way that the effects of annealing of ice at subzero temperature can be reduced or even compensated by keeping the sample subsequently at ambient temperature for increasing periods of time. The scans were obtained with a hydrated MetHb sample containing 0.50 (g water)/(g MetHb). Curves 1 and 2 were obtained in the same way as those in Fig. 1, i.e., the DSC heating curves were recorded at 30 K min^{-1} after cooling from 295 to 103 K at $\approx$150 K min^{-1} (curve 1) and after additional annealing at 258 K for 60 min (curve 2). For curve 3 the sample was cooled immediately after recording curve 2 from 295 to 103 K at $\approx$150 K min^{-1}, reheated, and its DSC scan taken. For each of curves 4–8, first an ice crystal size distribution similar to that of curve 2 was generated by repeating the procedure for curve 2, i.e., by cooling the sample from 295 to 103 K at $\sim$150 K min^{-1}, heating the sample to 258 K at 30 K min^{-1}, annealing the sample at 258 K for 60 min, cooling it, and reheating it to 298 K. After this procedure the sample was held at 298 K for increasing periods of time, cooled from 298 to 103 K at $\approx$150 K min^{-1}, reheated to 298 K at 30 K min^{-1}, and its DSC scan recorded. The isothermal period at 298 K was 1 min for curve 4, 10 min for curve 5, 60 min for curve 6, 120 min for curve 7, and 14 h for curve 8. This set of melting patterns shows that with increasing periods of isothermal holding time at ambient temperature the effects of annealing at subzero temperature seen in curve 2 are reduced, and that they are absent in curve 8, which is nearly identical to curve 1.

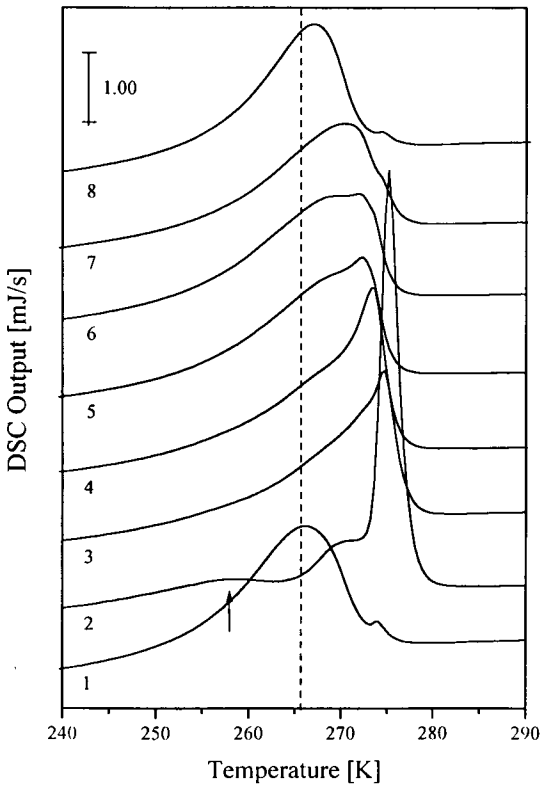

FIGURE 2 The effects of isothermal treatment at 295 K of a methemoglobin sample containing 0.50 (g water)/(g MetHb) on the melting pattern of ice for heating at a rate of 30 K min^{-1}. For curves 1 and 2 the sample was treated as for curves 1 and 2 of Fig. 1, i.e., cooled from 295 to 103 K at $\approx$150 K min^{-1}, heated, and its DSC scan taken (curve 1), and the procedure repeated but with additional annealing at 258 K for 60 min (curve 2). For curve 3 the sample was cooled immediately thereafter from 295 K to 103 K at $\approx$150 K min^{-1}, reheated, and its DSC scan taken. For each of curves 4–8, first an ice crystal size distribution similar to that of curve 2 was generated by repeating the procedure for curve 2, i.e., by cooling the sample from 295 to 103 K at $\approx$150 K min^{-1}, heating the sample to 258 K at 30 K min^{-1}, annealing the sample at 258 K for 60 min, cooling and reheating the sample to 298 K. After this procedure the sample was held at 298 K for increasing periods of time, cooled to 103 K at $\approx$150 K min^{-1}, reheated at 30 K min^{-1}, and its DSC scan taken. The isothermal period at 298 K was increased from curve 4 to curve 8 and was 1 min (curve 4), 10 min (curve 5), 60 min (curve 6), 120 min (curve 7), and 14 h (curve 8), respectively. Note in curves 4–8, with increasing holding time at 298 K, the increasing similarity of the melting patterns of the annealed sample to that of the unannealed sample in curve 1. The vertical broken line is at 266 K.

Fig. 3 demonstrates for a new sample of hydrated MetHb with 0.58 (g water)/(g MetHb) that annealing at subzero temperatures does not involve melting of ice. Curve 1 was obtained after cooling the sample from 298 to 103 K at $\approx$150 K min^{-1}, heating it at 30 K min^{-1} to 298 K, and recording its DSC scan. The broad asymmetric melting endotherm has

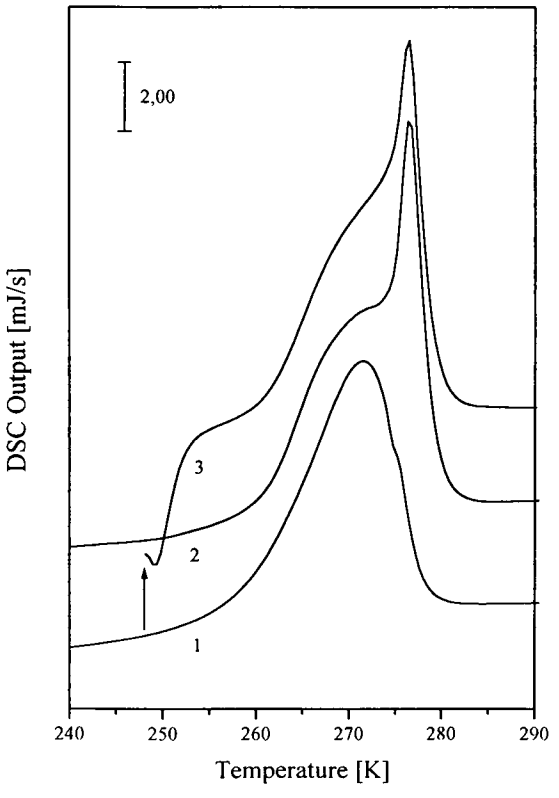

FIGURE 3 The DSC scans of the melting region of ice of a methemoglobin sample containing 0.58 (g water)/(g MetHb) for heating at a rate of 30 K min^{-1}. For curve 1 the sample was cooled from 298 K to 103 K at $\approx$150 K min^{-1}, heated to 298 K, and its DSC scan taken. Thereafter the sample was cooled for curve 2 from 298 to 103 K at $\approx$150 K min^{-1}, heated to 248 K at 30 K min^{-1}, annealed at 248 K for 60 min, cooled to 103 K at 30 K min^{-1}, reheated to 298 K, and its DSC scan taken. For curve 3 the sample was cooled thereafter from 298 to 103 K at $\approx$150 K min^{-1}, heated to 248 K at 30 K min^{-1}, annealed at 248 K for 60 min, reheated to 298 K at 30 K min^{-1}, and its DSC scan taken.

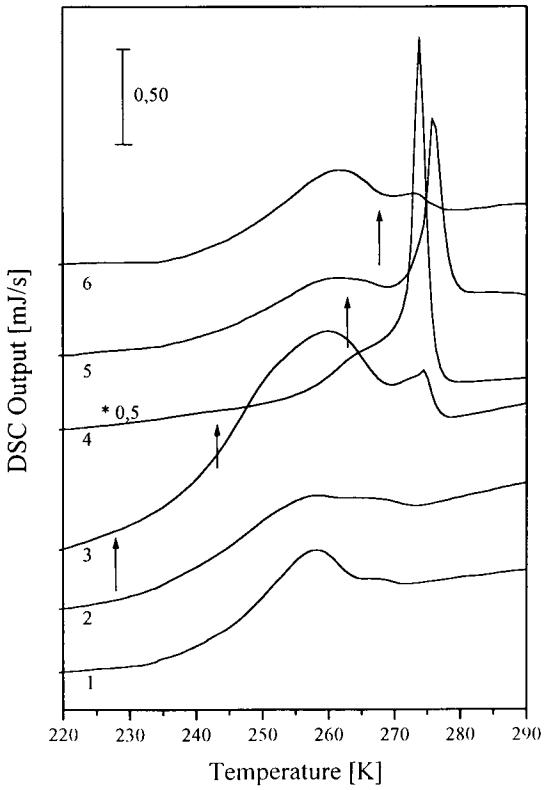

FIGURE 4 The effects of annealing temperature on the melting pattern of ice obtained with methemoglobin samples containing 0.43 (g water)/(g MetHb) and for heating at 30 K min^{-1}. For each curve a new sample was taken from the same batch. For curves 2–6, the sample was cooled from 298 to 103 K at ≈150 K min^{-1}, heated to the annealing temperature at 30 K min^{-1}, annealed at this temperature for 60 min, cooled to 103 K at 30 K min^{-1}, heated to 298 K at 30 K min^{-1}, and its DSC scan taken. The annealing temperature was 198 K (curve 2), 228 K (curve 3), 243 K (curve 4), 263 K (curve 5), and 268 K (curve 6), respectively. Curve 4 is shown at half size. Curve 1 shows for comparison the scan of the unannealed sample, which was cooled at ≈150 K min^{-1}, and then heated at 30 K min^{-1} and its DSC scan recorded.

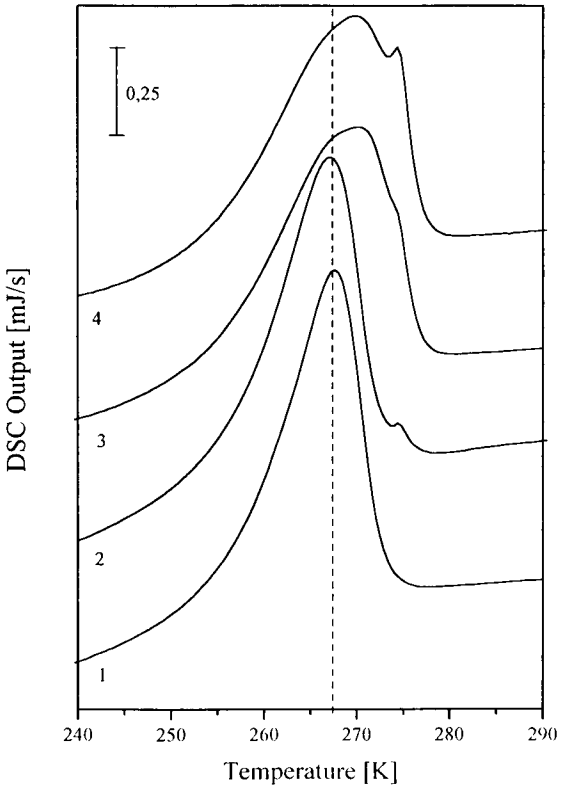

FIGURE 5 The effects of cooling rate on the melting pattern of ice obtained with a methemoglobin sample containing 0.50 (g water)/(g MetHb) and for heating at a rate of 30 K min^{-1}. For curves 1–4, the sample was cooled from 298 K to 103 K at ≈1500 K min^{-1} (curve 1), ≈150 K min^{-1} (curve 2), 10 K min^{-1} (curve 3), and 5 K min^{-1} (curve 4), respectively, and thereafter reheated at 30 K min^{-1} and its DSC scan recorded. The vertical broken line is at 267 K. The same sample was used first for Fig. 2.

a peak maximum at 270 K. For curve 2 the same sample was cooled from 298 to 103 K at ≈150 K min^{-1}, heated to 248 K at 30 K min^{-1}, annealed at 248 K for 60 min, cooled to 103 K at 30 K min^{-1}, and thereafter reheated at the same rate to 298 K and its DSC scan taken. A sharp endothermic peak centered at 275 K indicates ice crystal growth as an effect of annealing. For curve 3, the same sample was cooled to 103 K at ≈150 K min^{-1}, heated to 248 K at 30 K min^{-1}, annealed at 248 K for 60 min, and finally reheated to 298 K at 30 K min^{-1} and its DSC scan recorded. The wiggle at the beginning of this DSC scan is caused by a thermal gradient between sample and reference pan after start of the scan and is characteristic of DSC scans immediately after starting the scan. The area of the endotherms, obtained for integration from 256 to 284 K, is 40.5 J/(g sample) for curve 2 and 40.1 J/(g sample) for curve 3. This difference is within the accuracy of the DSC instrument.

This set of curves indicates that annealing at 248 K does not, or only to a minor extent, lead to melting of ice. Similar experimentation for higher annealing temperatures, e.g., for 258 K used for the DSC curves of Figs. 1 and 2, is not meaningful because the effects of thermal equilibration of the instrument overlap with the melting interval (which for integration of curve 2 was assumed to extend from 256 to 284 K, see above), and therefore, determination of the heat of melting is not possible.

Varying the annealing temperature for a given annealing time at subzero temperatures allows us to determine the onset temperature for the recrystallization and ice crystal growth process. This then can be compared with the influence of annealing temperature in the melting temperature region of ice. Fig. 4 shows DSC scans of MetHb samples containing 0.43 (g water)/(g protein), which were annealed at several temperatures in the range between 198 and 268 K for 60 min. For each curve a new sample was taken from the same batch. For curves 2–6 the sample was cooled from 298 to 103 K at ≈150 K min^{-1}, heated to the annealing temperature at 30 K min^{-1}, annealed at this temperature for 60 min, cooled to 103 K at 30 K min^{-1}, and heated to 298 K at 30 K min^{-1} while the DSC scan was taken. Curve 1 shows for comparison the DSC scan of an unannealed sample. In curve 1 a broad weak endothermic peak at 258 K indicates the melting of small ice crystals. For curves 2, 3, and 4, the sample was annealed at 198, 228, and 243 K, respectively. In curve 3, a second peak

due to the melting of larger ice crystals becomes observable at 273 K, which develops into the major peak in curve 4 (shown at half size). This peak is absent in curves 1 and 2.

For curves 5 and 6 of Fig. 4, the sample was kept isothermally at 263 and 268 K, respectively. The latter isothermal treatment is already within the temperature region where the ice melts, and it has the opposite effect to annealing at low temperatures in that the intensity of the peak at ≈273 K due to comparatively large ice crystals decreases in curve 5 and approaches in curve 6 that of curve 1.

In Fig. 5 the influence of cooling rate on the shape of the melting endotherm of ice is shown for a sample of MetHb containing 0.50 (g water)/(g MetHb). The vertical broken line is at 267 K. For curves 1–4, the sample was cooled from 298 to 103 K at ≈1500 (curve 1), ≈150 (curve 2), 10 (curve 3), and 5 (curve 4) K min^{-1}, respectively, and thereafter reheated at 30 K min^{-1} and its DSC scan taken. For curves 1 and 2, the shape and width of the dominant endotherm are very similar, and in curve 2 only a weak peak centered at ≈273 K of ≈1% total area indicates an influence of the decrease in cooling rate. For curves 3 and 4, however, the dominant melting endotherm clearly broadens and its maximum shifts to higher temperature, and the intensity of the component at ≈273 K increases. The area of the melting endotherms is for integration from 252 to 277 K 18.1 (curve 1) and 17.9 (curve 2), and for integration from 252 to 280 K 18.4 (curve 3) and 18.7 (curve 4) J/(g sample), respectively.

For Figs. 1–5 the samples were heated at most to 298 K. Higher temperatures than those where water had evaporated from the protein were also studied with the intention to be able to differentiate between the melting patterns of ice in the protein, and those of ice from evaporated water. In Fig. 6, for a MetHb sample with 0.50 (g water)/(g MetHb), we compare the shape of melting endotherms of the sample when heated to at most 298 K, with those of the same sample but heated to increasingly higher temperatures. The sample was cooled for each of the curves to 103 K at a rate of ≈150 K min^{-1}, reheated at a rate of 30 K min^{-1}, and its DSC scan taken. For curve 1 the sample was cooled from 298 K, heated, and its DSC scan taken. For curve 2 the cooling/heating cycle was repeated by cooling immediately after curve 1 and reheating. The similarity of melting patterns ascertains the reproducibility. For curve 3 the sample was heated after curve 2 to 358 K, immediately cooled, and reheated. For curve 4 the sample was heated after curve 3 to 368 K and immediately cooled and reheated. For curve 5 the sample was heated after curve 4 only to 298 K, kept at 298 K for 60 min, immediately cooled, and finally reheated and its DSC scan taken. The vertical broken line is at 275 K and indicates for curves 3–5 the peak maximum. Integration of the melting endotherms from 252 to 279 K for curves 1 and 2 and from 262 to 281 K for curves 3–5 gave 17.8 (curve 1), 17.7 (curve 2), 19.8 (curve 3), 21.1 (curve 4), and 19.5 (curve 5) J/(g sample), respectively. These values ascertain that the crimp-sealed aluminum pan did not leak and that no water had escaped during the heating/cooling cycles. Further heating/cooling cycles with another sample, with maximal temperatures of

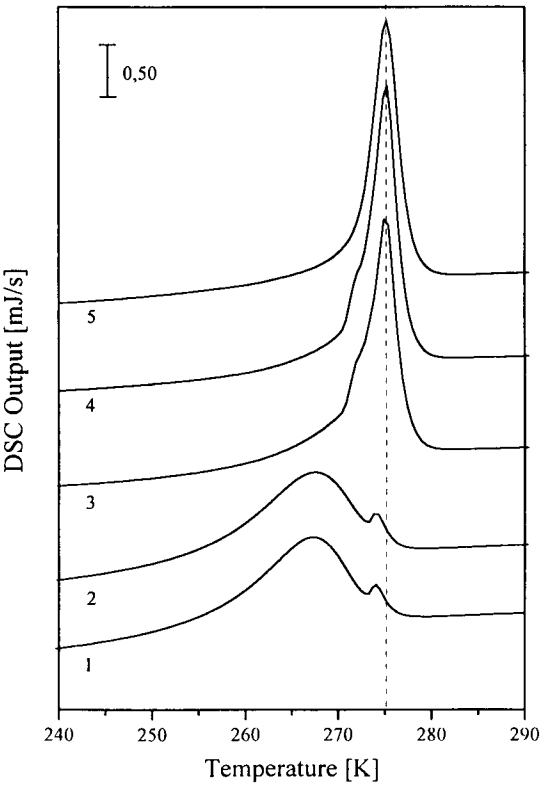

FIGURE 6 The effects of heating up to 368 K on the melting pattern of ice obtained with a methemoglobin sample containing 0.50 (g water)/(g MetHb). For curve 1 the sample was cooled from 298 to 103 K at ≈150 K min^{-1}, heated to 298 K at 30 K min^{-1}, and its DSC scan taken. For curve 2 the cooling/heating cycle of curve 1 was repeated for demonstrating the reproducibility. For curve 3 the sample was heated thereafter to 358 K, immediately cooled at ≈150 K min^{-1}, reheated at 30 K min^{-1}, and its DSC scan taken. For curve 4 the sample was heated thereafter to 368 K, immediately cooled to 103 K at ≈150 K min^{-1}, reheated at 30 K min^{-1} and its DSC scan taken. For curve 5 the sample was heated after curve 4 to 298 K, kept at 298 K for 60 min, cooled to 103 K at ≈150 K min^{-1}, reheated, and its DSC scan taken. The vertical broken line is at 275 K. The same sample was used first for Figs. 2 and 5 in this order.

308 and 318 K, gave on cooling and reheating from 103 K melting endotherms similar to those of curves 1 and 2 (not shown). We note that during heating of the sample to 358 and 368 K for curves 3 and 4 an intense endothermic feature is observable with an onset temperature of ≈≥340 K, which is mainly due to evaporation of water, and that this feature is absent during subsequent heating of the sample for curve 5 (not shown).

The reproducibility of the DSC scans shown in Figs. 1–5 was ascertained with samples taken from the same batch, and also with samples of another batch with slightly different hydration values.

DISCUSSION

We have first to ascertain that the melting patterns of ice shown in Figs. 1–5 are not obscured by an artifact due to evaporation of water from the hydrated protein and its condensation on the lid of the aluminum pan. This type of artifact

can occur because of a thermal gradient across the sample holder, and Franks et al. (1977) and Williams and Hirsh (1986) have argued that the double melting peak of ice frequently reported in the literature may be the result of condensation of water from the sample pan to the lid, which is somewhat cooler than the bottom of the pan. As a consequence, they consider that many of the variety of melting patterns reported for water-containing biological samples are caused by this artifact. Because of the artifact, in Fig. 6 we compare melting patterns of ice after heating of the sample at most to 298 K with those of the same sample, which had been heated to higher temperatures and where water had evaporated from the protein. We are confident that we can exclude this artifact as explanation for the various melting patterns shown in Figs. 1–5 for the following reasons. 1) In the melting patterns of curves 3–5 of Fig. 6, where water had evaporated upon heating to 358 or 368 K, the peak maximum of the intense peak is clearly shifted to higher temperature in comparison with the broad main peak of curves 1 and 2. It is also at a slightly higher temperature than the weak feature in curves 1 and 2 centered at 273 K. This is in line with the explanation of Williams and Hirsh (1986) that increasing condensation of water vapor on the lid of the aluminum pan leads upon cooling and reheating to increasing intensity of a melting endotherm shifted to higher temperature. Similar behavior was noted by Franks et al. (1977) for heating to 360 K. 2). For curve 5 of Fig. 6, isothermal treatment of the sample at 298 K for 60 min after its heating to 368 K for curve 4 had very little effect on the melting endotherm obtained after cooling and reheating of the sample. This is in clear contrast in particular to the curves of Fig. 2 where isothermal treatment for the same temperature and time causes pronounced changes in the melting patterns (see curve 6 of Fig. 2). Our interpretation of this is that, once water has evaporated from the protein, much longer times are necessary for its rehydration of the protein. 3) The melting patterns of hydrated MetHb samples cooled from 298 to 103 K at $\approx$150 K min^{-1} and heated at 30 K min^{-1} to 298 K without prior annealing are highly reproducible and are independent of the holding time at 298 K. If evaporation of water from the hydrated protein and its condensation on the lid of the sample pan was to occur at 298 K, one would expect with increasing holding time at 298 K increasing intensity of the melting peak at higher temperature. 4) In Figs. 1–5, the intensity of the sharp melting peak with a maximum at $\approx$273 K is most pronounced after annealing at subzero temperatures, for example at 248 (curve 4 of Fig. 4) or 258 K (curve 2 of Fig. 1). However, at these temperatures the vapor pressure of ice is lower by more than an order of magnitude than that of water at 298 K, and therefore, at subzero temperatures sublimation of ice from the protein to the lid during annealing is unlikely. We conclude that heating to at most 298 K is a safe temperature for avoiding, for the hydration range used in this study, evaporation of water from the protein and development of the artifact.

This study developed out of our previous study of the glass→liquid transition and crystallization behavior of the vitreous but freezable water fraction in hydrated MetHb, and the basic results of that study must be briefly mentioned for better understanding of this work (Sartor et al., 1992, 1993). Water in hydrated MetHb powders, with water content of between 0.43 and 0.58 (g water)/(g MetHb) used in this study, is according to x-ray diffractograms completely vitrified on cooling at a rate of $\approx$150 K min^{-1} (see Fig. 1 in Sartor et al., 1992, 1993). MetHb samples with higher water content than those used here require increasing rates of cooling for complete vitrification, but were not used first because of experimental difficulties, and second because the melting patterns of these samples increasingly resemble that of "bulk" ice and effects of annealing at subzero temperatures become less obvious. The effect of water content on the melting curves of unannealed samples is seen already from a comparison of Fig. 4 with the other figures because the sample used for Fig. 4 contained 0.43 (g water)/(g MetHb) and the peak maximum of the unannealed sample was at $\sim$258 K (curve 1), whereas for the other figures the samples contained $\geq$ 0.50 (g water)/(g MetHb) and the maximum shifted to $\sim$268 K.

The vitrified, but freezable, water fraction shows on reheating at a rate of 30 K min^{-1} a glass→liquid transition with an onset temperature, or T_g, at 169 $\pm$ 2 K, and starts to crystallize to cubic ice at $\approx$210 K, which then starts to transform to hexagonal ice at $\approx$240 K. These temperatures are for samples kept isothermally at each temperature for $\approx$½ h for taking its diffractogram, and they must be shifted to a higher temperature for heating at a rate of 30 K min^{-1}. Therefore, it is conceivable that for this heating rate at 240 K, which is the low temperature end of Figs. 1–6, ice is present in its cubic form, which on further heating either first transforms to hexagonal ice and/or melts as cubic ice. The cubic to hexagonal ice phase transition would then be superimposed on the melting of ice, but it would not be noticeable because for bulk cubic ice the heat of transformation to hexagonal ice is only $\approx$50 J mol^{-1} (Handa et al., 1988). However, in samples cooled at 10 K min^{-1}, the water fraction transforms completely to hexagonal ice already on cooling (Fig. 2 in Sartor et al., 1992). Therefore, for the samples cooled here at a rate of $\geq\approx$150 K min^{-1}, we can safely assume that the water has been vitrified, but for the sample cooled at $\leq$10 K min^{-1}, the freezable water fraction must have transformed during cooling into hexagonal ice.

In the interpretation of the DSC melting patterns we have to differentiate clearly between the effects of annealing at subzero temperatures and those of keeping the sample isothermally at ambient temperature or within the temperature region of the melting endotherm. The effect of annealing at subzero temperatures, which is seen most clearly in curve 2 of Fig. 1 for annealing at 258 K and in curve 4 of Fig. 4 for annealing at 248 K, is attributed to recrystallization of the small ice crystals formed on heating from the vitreous state at 30 K min^{-1} up to the annealing temperature into larger ones during annealing. This results in a shift of the melting temperature of ice to higher temperatures according to the Gibbs-Thomson equation (Pruppacher and Klett, 1980), and

can be observed in the DSC melting patterns of this study by development of an intense sharp endotherm with a peak maximum of ≈273–275 K. Development of a second broad melting peak at ≈270 K, which is observable in some of the melting curves of annealed samples as a shoulder, indicates formation of a second fraction of recrystallized ice that must be of smaller size than that melting at ≈273 K. The interpretation is supported by curves 2 and 3 of Fig. 3 where for annealing at 248 K for 60 min it is shown that during this treatment very little or no ice can have melted. These "large" ice crystals formed during annealing melt on heating into water clusters that must be of a larger size than those present in the equilibrated sample before first cooling. We note that the endothermic shoulder seen, e.g., in curve 4 of Fig. 4 at ≈270 K and assigned to the melting of an ice fraction, cannot, or only can to a minor extent, be caused by enthalpy relaxation of the unfreezable water fraction of hydrated MetHb, because this feature is much more intense than those reported by Sartor et al. (1994).

Crystal growth of ice during annealing at subzero temperatures could be followed more directly by x-ray diffraction because the half bandwidth of the reflections decreases with increasing crystal size according to the Scherrer formula (West, 1985). However, the quality of our x-ray powder diffractometer is not sufficient to make the necessary corrections for determining half bandwidth and ice crystal size. But, for a sample of MetHb containing 0.50 (g water)/(g MetHb) sharpening of the reflections with increasing temperature is seen in Fig. 1 of Sartor et al. (1992)

Immediately after melting of the "large" ice crystals formed during annealing, a nonequilibrium distribution of "large" water clusters in the protein is present. The effects of keeping the sample isothermally at ambient temperature can then be understood in terms of the redistribution and apparent equilibration of these "large" water clusters in the protein into smaller ones as a function of time. The effect of increasing the time for isothermal treatment at 298 K on the melting pattern of ice is seen most clearly in Fig. 2 where in curves 1 and 2 the two extremes, namely the melting patterns of the apparently equilibrated (curve 1) and of the annealed (curve 2) sample are shown, and where in curves 3–8 the melting patterns increasingly resemble that of curve 1 with increasing isothermal treatment at 298 K. Isothermal treatment in the melting temperature region or repeated cooling/heating cycles have a similar effect. For the former, curves 5 and 6 of Fig. 4 show that annealing at 263 or 268 K, respectively, has the effect of increasingly reducing the intensity of the peak at 273 K caused by large ice crystals. For the latter, curve 3 of Fig. 1 shows that a further cooling/heating cycle also can reduce the intensity of the peak at 273 K at the expense of the peak at lower temperature. This can be continued, and after several further cooling/heating cycles the melting pattern approaches that of curve 1 in Fig. 1. We note that a clusterwise mechanism of bound water melting has been suggested by Goldanskii and Krupyanskii (1989) to explain experimental data on hydrated proteins obtained by Rayleigh scattering of Mössbauer radiation.

This study can give us, first, a temperature range for the onset and extent of recrystallization at subzero temperatures, and second, a time scale for apparent equilibration and redistribution of the "large" water clusters on the protein into smaller ones at ambient temperature. Fig. 4 shows that, by taking development of a melting peak at ≈273 K as indicator for recrystallization and crystal growth, recrystallization does not occur during annealing at 198 K (curve 2), becomes noticeable at 228 K (curve 3), and is very pronounced at 243 K (curve 4). These temperatures have to be compared with other values for recrystallization of ice which were obtained mainly in cryoelectron microscopic studies. Robards and Sleytr (1985, p. 19) conclude that "recrystallization probably does not take place at significant rates until the temperature is above 180–190 K." This is consistent with our observations.

Second, the time scale necessary for apparent equilibration at 298 K can be deduced from the melting endotherms of Fig. 2. Effects are noticeable even in going from curve 2 to 3, where only a further cooling/heating cycle was done, but it requires more than 2 h until in curve 8 the melting pattern is nearly superimposable with that of curve 1.

After interpretation of the DSC curves shown in Figs. 1–4, the effect of cooling rate on the melting pattern of ice shown in Fig. 5 for a hydrated MetHb sample with 0.52 (g water)/(g MetHb) seems clear to us. For curves 1 and 2 obtained after cooling the sample at ≈1500 and 150 K min^{-1} and reheating at 30 K min^{-1}, the shape of the dominant melting endotherm is nearly identical. Only a weak peak centered at 273 K of ≈1% of the total area indicates in curve 2 formation of a small fraction of ice of larger crystal size. For both cooling rates and the hydration value used here, x-ray diffractograms have established complete vitrification of the vitreous but freezable water fraction (see Fig. 1 in Sartor et al., 1992, 1993). It is possible that in curve 2 the weak peak at ≈273 K is due to formation of ice formed already during cooling at ≈150 K min^{-1}, and this small amount of ice would not have been observable in the x-ray diffractograms. For curves 3 and 4 the sample was cooled at 10 and 5 K min^{-1}: for these rates of cooling, the vitreous but freezable water fraction transforms on cooling completely into hexagonal ice (see Fig. 2 in Sartor et al., 1992). The melting curves obtained on reheating at 30 K min^{-1} show considerable broadening and shift of the major endotherm to higher temperature, and increasing intensity of the component at ≈273 K, both indicating larger ice crystal size distributions for melting curves 3 and 4 than for curves 1 and 2.

The melting curve patterns of Fig. 5 enable us to address the question whether or not during vitrification of the vitreous but freezable water fraction by rapid cooling the water molecules occupy the same positions at ambient and at cryogenic temperatures, or if clustering of the water molecules occurs already during cooling. This question is of general importance for any attempt to use measurements taken at subambient temperatures to interpret the behavior at ambient temperature, and it has been argued that this approach might not necessarily be meaningful (Kuntz and Kauzmann, 1974;

Rupley and Careri, 1991). A comparison of the melting curves 1 and 2 obtained for cooling at rates of ≈1500 and ≈150 K/ min^{-1} shows that except for the weak peak at ≈273 K in curve 2, the melting patterns are nearly identical. Considering the sensitivity of the melting endotherms to clustering of water and ice crystal growth shown in this study, we conclude that the similarity of these two melting endotherms indicates similar distribution of water on cooling, and of ice crystal size on reheating. We further surmise that this similarity of the two melting curves, observed despite changes in cooling rate by about one order of magnitude, can be taken as an indication that for this range of hydration during cooling at rates of ≥≈150 K min^{-1} the distribution of water molecules present at ambient temperature on the whole does not change. This is consistent with Teeter's (1991) observation that for crystals of the protein crambin "flash-cooled" to 130 K, many of the water positions at 130 K correspond almost exactly to what is seen at 300 K.

The size of the ice crystals in unannealed samples, its increase during annealing at subzero temperatures, and the size of the water clusters formed subsequently on melting of the ice, are important for an understanding of the dynamics of the water molecules and the rate of redistribution and apparent equilibration at ambient temperature, and it could give us an idea where the vitreous but freezable water fraction characterized in this study and the previous one can be located. It can in principle be determined by the Gibbs-Thomson equation. Pruppacher and Klett (1980) display in their Figs. 6–8 numerical solutions of the Gibbs-Thomson equation: in the case of an ice particle in a supercooled solution drop in humid air, the variation of equilibrium freezing temperature with drop size, ice particle size and concentration of NaCl in solution is shown. The equilibrium freezing temperature is seen to decrease with decreasing size of the ice particle, and this decrease is further enhanced by the solute effect if the salt concentration is larger than ≈0.1 M. We briefly discuss several sizes of ice particles: for pure water and dilute solutions, the equilibrium freezing point depression, or ΔT, is ≈16°C for an ice sphere radius of 30 Å, ≈23°C for a radius of 20 Å, and approaches for radii ≥100 Å within a few degrees the triple point for bulk phases (read from Figs. 6–8 of Pruppacher and Klett, 1980). These values are consistent with those recently reported by Handa et al. (1992), where the effect of restricted geometries on the structure and thermodynamic properties of ice was investigated and ΔT values of ≈20°C for ice in pores of 23 Å pore radius, and of ≈7°C for ice in pores of Vycor glass of pore radius of ≈42 Å was obtained. The onset temperature of the main melting peak of ice observed in this study for hydrated MetHb samples cooled at ≥≈150 K min^{-1} and heated without prior annealing is difficult to determine because of the gradual change of slope, and it could be anywhere between 247 and 253 K (see, e.g., curve 1 in Fig. 1 and curves 1 and 2 in Fig. 5). The average value of ΔT of ≈23°C would for pure water correspond to an ice sphere radius of ≈20 Å and could be taken as an indication for the size of the ice crystal formed on heating the vitreous but freezable water. However, these values need not be the same for water, and ice, in a protein.

In our previous study of the vitreous but freezable water fraction in hydrated MetHb (Sartor et al., 1992, 1993) we have argued that this water fraction either might form a second hydration shell or might be enclosed in the holes and/or loops of the protein's chains, and we have tentatively preferred the latter because of the remarkable similarity of its glass→liquid transition and crystallization behavior with that of water embedded in the pores of a synthetic hydrogel (Hofer et al., 1990). In a review of the structure and dynamics of water surrounding biomolecules, Saenger (1987, p. 100) "distinguishes two kinds of water molecules associated with proteins: water at the periphery, which provides the hydration shell, and internal water, which fills cavities in the protein and diminishes local charge-charge interactions." He further points out that in all proteins containing internal water, these water molecules are so mobile that they exchange easily with bulk water. This mobile exchange is a prerequisite for our tentative assignment of the vitreous but freezable water to water in the pores and/or loops of the protein's chains, and for crystal growth of ice at subzero temperatures and subsequent redistribution and apparent equilibration at ambient temperature.

The next step is to understand the macroscopic effects, obtained in this study by an indirect technique, on a molecular level and to connect it with the many microscopic studies of the dynamics of water in hydrated proteins by so-called direct techniques. This can be done by following redistribution and apparent equilibration of the large water clusters at ambient temperatures, after generating a nonequilibrium distribution by crystal growth at subzero temperatures, as a function of time and/or temperature by, e.g., NMR spectroscopy. Of the many NMR spectroscopic studies we mention only the recent work by Kimmich and co-workers (Kimmich et al., 1990; Kimmich, 1993) where highly dynamic exchange between water of hydration and additional or "free" water has been reported from NMR studies of water diffusion in hydrated bovine serum albumin. Kimmich (1993) differentiates between three concentration ranges, and for range II of ≈50 < wt % protein < ≈85, which includes the hydration range used in this study, they speak of the "infinite-cluster regime" where the hydration shells are in close contact with one another. This rapid exchange is a necessary condition for our suggestion that the vitreous but freezable water fraction is located in pores and/or loops of the protein's chains (Sartor et al., 1992, 1993), and it allows ice crystal growth at subzero temperatures and its redistribution and apparent equilibration at ambient temperature. The time scale for redistribution and apparent equilibration of the "large" water clusters formed on melting of recrystallized ice (compare, e.g., Fig. 2, curves 7 and 8) seems to be much longer than expected for the high mobility of hydration water because for this hydration range the diffusion coefficient within the hydration shells is only one order of magnitude less than that of bulk water (Kimmich, 1993). This

suggests that perturbation of the distribution of water molecules by ice crystal growth is large, and that redistribution and apparent equilibration at ambient temperature proceeds via many intermediate steps.

Finally we briefly address the question of whether crystal growth of ice at subzero temperatures and redistribution of the water clusters at ambient temperature have an effect on the protein itself. Evidence for coupling of internal motions of the protein with the adjacent solvent is manifold, and Rupley and Careri (1991) discuss and review these. The two types of changes in the solvent distribution described in this study are expected to lead to changes in H-bond interaction of the water, and ice, with the protein surface. We do not expect large changes in the protein's structure because even for the hydration range of 0.07–0.4 (g water)/(g protein) the changes are small (see Table VII in Rupley and Careri, 1991). Nevertheless, subtle changes seem possible and could be investigated by, e.g., NMR spectroscopy.

We are grateful for financial support by the Forschungsförderungsfonds of Austria (project P10404-PHY).

REFERENCES

Cooke, R., and I. D. Kuntz. 1974. The properties of water in biological systems. *Annu. Rev. Biophys. Bioeng.* 3:95–125.

Doster, W., A. Bachleitner, R. Dunau, M. Hiebl, and E. Lüscher. 1986. Thermal properties of water in myoglobin crystals and solutions at subzero temperatures. *Biophys. J.* 50:213–219.

Finney, J.L. 1986. The role of water perturbations in biological processes. *In* Water and Aqueous Solutions. G. W. Neilson and J. E. Enderby, editors. Colston papers No 37, Adam Hilger, Bristol. 227–244.

Franks, F., M. H. Asquith, C. C. Hammond, H. L. B. Skaer, and B. Echlin. 1977. Polymeric cryoprotectants in the preservation of biological ultrastructure. *J. Microsc.* 110:223–238.

Goldanskii, V. I., and Y. F. Krupyanskii. 1989. Protein and protein-bound water dynamics studied by Rayleigh scattering of Mössbauer radiation. *Q. Rev. Biophys.* 22:39–92.

Hallbrucker, A., E. Mayer, and G. P. Johari. 1989. The heat capacity and glass transition of hyperquenched glassy water. *Philos. Mag.* 60B:179–187.

Handa, Y. P., D. D. Klug, and E. Whalley. 1988. Energies of the phases of ice at low temperature and pressure relative to ice Ih. *Can. J. Chem.* 66:919–924.

Handa, Y. P., M. Zakrzewski, and C. Fairbridge. 1992. Effect of Restricted Geometries on the Structure and Thermodynamic Properties of Ice. *J. Phys. Chem.* 96:8594–8599.

Hofer, K., E. Mayer, and G. P. Johari. 1990. Glass-liquid transition of water and ethylene glycol solution in poly(2-hydroxyethyl methacrylate) hydrogel. *J. Phys. Chem.* 94:2689–2696.

Johari, G. P., A. Hallbrucker, and E. Mayer. 1987. The glass transition of hyperquenched water. *Nature.* 330:552–553.

Kimmich, R., T. Gneiting, K. Kotitschke, and G. Schnur. 1990. Fluctuations, exchange processes, and water diffusion in aqueous protein systems. *Biophys. J.* 58:1183–1197.

Kimmich, R. 1993. Self-diffusion and NMR relaxation in hydration shells of proteins. *In* Water-Biomolecule Interactions, Conference Proceedings, Vol. 43. M. U. Palma, M. B. Palma-Vittorelli and F. Parak, editors. Società Italiana di Fisica, Bologna. 157–164.

Kuntz, I. D., and W. Kauzmann. 1974. Hydration of proteins and polypeptides. *Adv. Protein Chem.* 28:239–345.

Poole, P. L., and J. L. Finney. 1986. Solid-phase protein hydration studies. *Methods Enzymol.* 127:284–293.

Pruppacher, H. R., and J. D. Klett. 1980. Microphysics of Clouds and Precipitation. D. Reidel Publishing Company, Dordrecht, Holland. 149–161.

Robards, A. W., and U. B. Sleytr. 1985. Low Temperature Methods in Biological Electron Microscopy. Elsevier, Amsterdam. 5–19.

Rupley, J. A., and G. Careri. 1991. Protein hydration and function. *Adv. Protein Chem.* 41:37–172.

Saenger W., 1987. Structure and dynamics of water surrounding biomolecules. *Annu. Rev. Biophys. Biophys. Chem.* 16:93–114.

Sartor G., A. Hallbrucker, K. Hofer, and E. Mayer. 1992. Calorimetric glass-liquid transition and crystallization behavior of a vitreous, but freezable, water fraction in hydrated methemoglobin. *J. Phys. Chem.* 96: 5133–5138.

Sartor, G., A. Hallbrucker, K. Hofer, and E. Mayer. 1993. Glass-liquid transition and crystallization of a vitreous but freezable water fraction in hydrated methemoglobin. *In* Water-Biomolecule Interactions, Conference Proceedings Vol. 43. M. U. Palma, M. B. Palma-Vittorelli and F. Parak, editors. SIF, Bologna. 143–146.

Sartor, G., E. Mayer, and G. P. Johari. 1994. Calorimetric studies of the kinetic unfreezing of molecular motions in hydrated lysozyme, hemoglobin, and myoglobin. *Biophys. J.* 66:249–258.

Teeter, M. M. 1991. Order and disorder in water structure of crystalline proteins. *Dev. Biol. Standard.* 74:63–72.

Waterman, M. R. 1978. Spectral characterization of human hemoglobin and its derivatives. *Methods Enzymol.* 52:456–463.

West, A. R. 1985. Solid State Chemistry and its Applications. Wiley, New York. 173–175.

Williams, R. J., and A. G. Hirsh. 1986. On the freezing of water and melting of ice in scanning calorimeters. *Cryo Lett.* 7:146–161.

Wunderlich, B. 1990. Thermal Analysis. Academic Press, Boston. 186–202.